Monatshefte für Chemie 136, 1157–1169 (2005)
DOI 10.1007/s00706-005-0292-0

Monatshefte für Chemie
Chemical Monthly
Printed in Austria

Synthesis and Properties of Mononuclear and Homobinuclear Chelates of Mn(II), Co(II), Ni(II), and Cu(II) with Phthalein Purple

Kamal Y. El-Baradie[1,*], **Tarek M. Fayed**[1], and **Ibrahim M. El-Mehasseb**[2]

[1] Chemistry Department, Faculty of Science, Tanta University, Tanta, Egypt
[2] Chemistry Department, Faculty of Education (Kafr El-Sheikh), Tanta University, Kafr El-Sheikh, Egypt

Received September 18, 2004; accepted (revised) October 20, 2004
Published online March 21, 2005

Summary. Mono- and homobinuclear complexes of Mn(II), Co(II), Ni(II), and Cu(II) with phthalein purple are prepared and characterized by elemental analysis, thermal studies (TGA and DTA), spectral methods (IR, UV/Vis, and ESR), magnetic moment determination, and electrochemical reduction (DC polarography at DME and CV at HMDE). Thermal degradation of the complexes was studied by TGA and DTA where some thermodynamic parameters were determined. The mode of bonding and geometry of the complexes were determined from the spectral studies. Magnetic moment values showed some antiferromagnetism in the homobinuclear complexes. The reduction of the metal ions proceeds to the metallic state along an irreversible process.

Keywords. Phthalein purple; Complexes; Electronic spectra; Magnetic measurement.

Introduction

Phthalein purple (*PhP*, also known as *ortho*-cresol phthalein complexone) is generally used as a chromogenic reagent for the spectrophotometric determination of many metal ions such as Mg(II), Ca(II), Ba(II), Sr(II), and Zn(II) [1–5]. Also *PhP* found wide applications in high-performance chelation ion chromatography involving dye-coated resins used for determination of alkali and alkaline earth metals as well as many transition metal ions like Mn(II), Co(II), Cd(II), Zn(II), Ni(II), and Cu(II) [6–8]. The acid-base properties and the complexing stability of *PhP* towards some metal ions in solution were also studied by *pH*-metric method [9]. The pK_a values were given and the formation of 1:1 and 2:1 (M^{x+}:ligand) complexes were reported.

* Corresponding author. E-mail: kyelbaradie@hotmail.com

Despite the fact that the reaction of *PhP* with several metal ions in solution was the subject of several interesting studies, yet to the knowledge of the authors no detailed study of its metal complexes in the solid state has been carried out. Binuclear metal complexes are of special interest in the field of bio- and analytical chemistry. Many proteins were found to improve their activity in the presence of bi- or poly-nuclear metal complexes [10, 11]. Emocyanine is an enzyme containing a binuclear copper(II) complex that acts as an active site for the activation of oxygen [12–14].

In the present investigation, it is attempted to prepare and characterize the mononuclear and binuclear Mn(II), Co(II), Ni(II), and Cu(II) with *PhP* using elemental and thermal analyses as well as spectral methods (IR, UV/Vis, and ESR) together with magnetic moment determination and electrochemical reduction. This stemed from the fact that the solid metal complexes of *PhP* have not been well investigated.

Results and Discussion

The stoichiometry of the solid complexes was firstly confirmed by elemental analysis for the isolated chelates (Table 1). The elemental analysis data show satisfactory agreement with the suggested formulae.

Thermal Analysis

The results of thermogravimetric analysis (Table 2) indicate that the dehydration of the complexes and their decomposition proceed mainly in three steps. For Mn(II)

Table 1. Chemical formulae and physical properties, of complexes

No.	Formula of compound	Colour (Formula wt)	μ_{eff} / BM · metal ion	g_{eff} (ESR value)
1	$[MnL3H_2O]H_2O$ $C_{32}H_{38}N_2O_{16}Mn$	Beige (760.93)	5.80	1.951
2	$[Mn_2L6H_2O]2H_2O$ $C_{32}H_{44}N_2O_{20}Mn_2$	Beige (885.86)	5.20	1.951
3	$[CoLH_2O]H_2O$ $C_{32}H_{34}N_2O_{14}Co$	Blue-green (728.93)	4.14	2.1372
4	$[Co_2L2H_2O]2H_2O$ $C_{32}H_{36}N_2O_{16}Co_2$	Blue (821.86)	3.15	2.5150
5	$[NiLH_2O]H_2O$ $C_{32}H_{34}H_2O_{14}Ni$	Yellowish green (728.7)	d	–
6	$[Ni_2L2H_2O]2H_2O$ $C_{32}H_{36}N_2O_{16}Ni_2$	Olive green (821.4)	d	–
7	$[CuLH_2O]$ $C_{32}H_{32}N_2O_{13}Cu$	Pale green (715.54)	1.74	2.1413
8	$[Cu_2L2H_2O]$ $C_{32}H_{32}N_2O_{14}N_2Cu_2$	Dark green (795.88)	1.63	2.1617

$L = PhP$ – ligand; d = diamagnetic

Table 2. Results of thermogravimetric analysis of mononuclear and binuclear Mn(II) and Co(II) complexes

No.	Formula wt of the complex or the decomposition product	Process	Temperature range/°C	Product	Mass loss/%	
					Found	Calcd
1	$[MnL3H_2O]H_2O$ 760.93	Loss of water of hydration	30–120	H_2O	2.3	2.4
	$[MnL3H_2O]$ 742.93	Loss of coordinated water	120–240	$3H_2O$	7.3	7.1
	[Mn*L*] 688.93	Loss of amine part + two methyl groups	240–440	Amine part+CH_4	30.5	30.9
	Degradation of whole molecule and formation of manganese oxalate (440–650°C)					
2	$[Mn_2L6H_2O]2H_2O$ 885.86	Loss of water of hydration	30–120	$2H_2O$	4.3	4.1
	$[Mn_2L6H_2O]$ 849.86	Loss of coordinated water	120–260	$4H_2O$	12.4	12.2
	$[Mn_2L]$ 741.86	Loss of phthalein part + two acetate groups	260–460	Phthalein part+two acetic acid	24.6	24.8
	Degradation of whole molecule and formation of manganese oxalate (460–700°C)					
3	$[CoLH_2O]H_2O$ 728.93	Loss of water of hydration	40–120	H_2O	2.4	2.5
	$[CoLH_2O]$ 710.93	Loss of coordinated water	120–190	$3H_2O$	2.5	2.5
	[Co*L*] 692.93	Loss of amine part + two methyl groups	190–450	Amine part+CH_4	32.4	31.8
	Degradation of whole molecule and formation of cobalt oxalate (450–750°C)					
4	$[Co_2L2H_2O]2H_2O$ 821.86	Loss of water of hydration	30–110	$2H_2O$	4.3	4.4
	$[Co_2L2H_2O]$ 789.86	Loss of coordinated water	110–220	$4H_2O$	4.7	4.4
	$[Co_2L]$ 753.86	Loss of phthalein part + two acetate groups	220–460	Phthalein part+two acetic acid	27.1	26.5
	Degradation of whole molecule and formation of cobalt oxalate (460–800°C)					

mononuclear complex **1**, the first weight loss within the temperature range 30–120°C, which is associated with an endothermic peak at 73°C in the DTA thermogram, is attributed to the loss of lattice water molecules. The second step which takes place within the temperature range 120–240°C, with an endothermic peak at 173°C, is reasonably accounted for the elimination of coordinated water molecules. The third step 240–440°C), with an exothermic peak at 398°C, is attributed to the loss of one amine part and the two methyl groups from the cresol rings leaving manganese oxalate as a final product. The thermogram of homobinuclear Mn(II) complex **2**

shows that the two lattice water molecules are eliminated within the temperature range 30–120°C with an endothermic peak at 110°C. The second step (160–260°C) involves the loss of coordinated water molecules. This step is associated with an exothermic peak at 195°C. The third step of decomposition (260–460°C), associated with an exothermic peak at 343°C, corresponds to the loss of the phthalein part and the two non-complexed acetate groups followed by further decomposition of the complex leaving behind manganese oxalate as a final product.

The mononuclear Co(II) complex **3** was thermally decomposed in different steps as supported by the DTA data. The first step, in the range 40–120°C, corresponds to loss of lattice water of the complex. This step is correlated with an endothermic peak at 81°C in the DTA themogram. In the second step, the elimination of coordinated water molecules takes place in the temperature range 120–190°C. This step is confirmed by the presence of an endothermic peak at 183°C. This is followed by the elimination of one amine part and the two methyl groups in the temperature range 190–450°C, with an exothermic peak at 320°C. Finally, the decomposition step within the temperature range 450–750°C, which is associated with an exothermic peak at 519°C, corresponds to the decomposition of the ligand molecule leading to cobalt oxalate as a final product. The thermogram of homobinuclear Co(II) complex **4** shows that the loss within the temperature range 30–110°C is due to removal of lattice water molecules which is associated with an endothermic peak at 90°C. The second step within the temperature range 110–220°C is associated with an endothermic peak at 175°C, and is due to the loss of coordinated water molecules. The third step of decomposition, in the temperature range 220–460°C with an exothermic peak at 368°C, may be attributed to the loss of the phthalein part and two acetate groups. The final stage of decomposition occurs within the temperature range 460–800°C and corresponds to the complete loss of the organic moiety leading to cobalt oxalate as a final product.

The IR spectra of the decomposition products of the complexes heated between 450–650°C for about 60 minutes were examined with the aim of confirming the structure of the final decomposition product. The spectra show bands at 1700–1640 cm^{-1} [υ(C=O)], 1420–1360 cm^{-1} [υ(C–O)], and 510–460 cm^{-1} [ring deformation + δ(O–C–O)], characteristic of metal oxalate [13].

The order n and activation energy E^* of the decomposition steps were determined using *Coats-Redfern* equation (Eqs. (1) and (2)) [16].

$$\ln\left[\frac{1-(1-\alpha)^{1-n}}{(1-n)T^2}\right] = M/T + B \quad \text{for } n \neq 1 \tag{1}$$

$$\ln\left[\frac{-\ln(1-\alpha)}{T^2}\right] = M/T + B \quad \text{for } n = 1 \tag{2}$$

where $M = -E^*/\mathrm{R}$ and $B = \ln \mathrm{AR}/\Phi\ E^*$; E^*, R, A, and Φ are the activation energy, gas constant, pre-exponential factor, and the heating rate respectively. The correlation coefficient, r, is calculated using the least squares method for different values of n. The left hand side of Eqs. (1) and (2) for *Coats–Redfern* method was plotted against $1000/T$ (Figs. 1 and 2). From the intercept and the slope of each stage, the A and E^* values were determined. The other kinetic parameters (ΔH^*, ΔS^*, and ΔG^*) were calculated using the relationships:

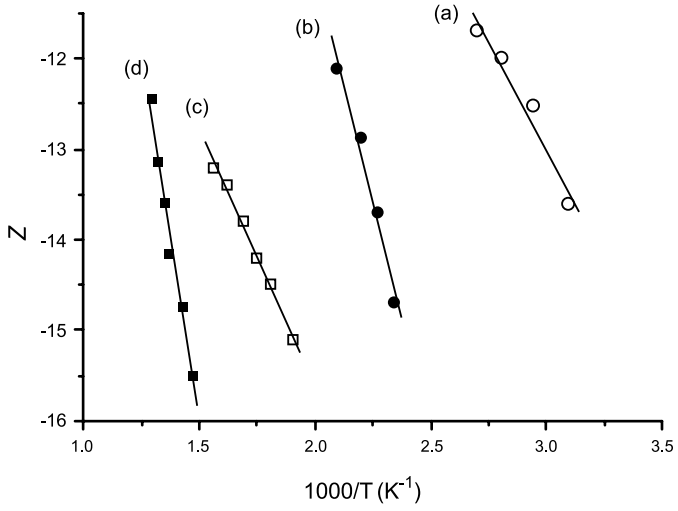

Fig. 1. *Coats-Redfern* plots for complex **1**; (a) first step, (b) second step, (c) third step, and (d) fourth step; $Z = \ln[(1-1-\alpha)^{1-n}/T^2(1-n)]$ for $n \neq 1$, or $Z = \ln[-\ln(1-\alpha)/T^2]$ for $n = 1$

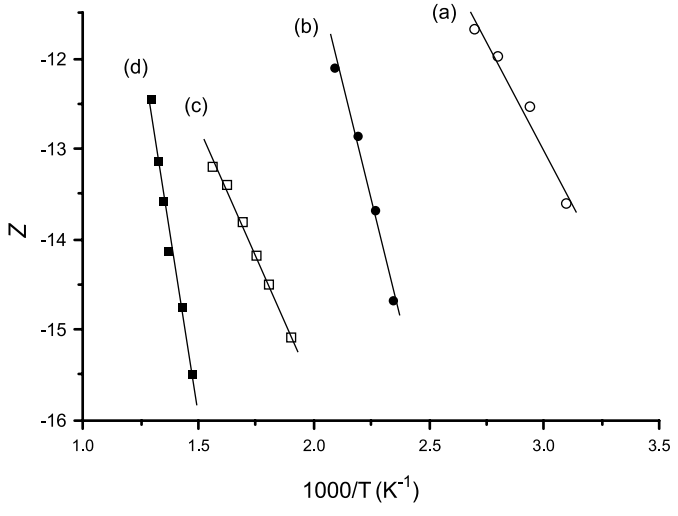

Fig. 2. *Coats-Redfern* plots for complex **3**; (a) first step, (b) second step, (c) third step, and (d) fourth step; $Z = \ln[(1-1-\alpha)^{1-n}/T^2(1-n)]$ for $n \neq 1$, or $Z = \ln[-\ln(1-\alpha)/T^2]$ for $n = 1$

$\Delta H^* = E^* - RT$, $\Delta S^* = R\ [\ln(Ah/kT) - 1]$, and $\Delta G^* = \Delta H^* - T\Delta S^*$, where k is *Boltzmann*'s constant and h is the *Planck*'s constant. The order and kinetic parameters of the decomposition of complexes are listed in Tables 3 and 4. The ΔS^* values were found to be negative which indicate that the activated complex is more ordered than the reactant and/or the thermal decomposition reaction is slower than normal. ΔG^* values increase with increasing the order of the decomposition stages which indicates that at high temperatures the ligand decomposes and requires more energy for its rearrangement in the activated

Table 3. Values of correlation coefficient, slope, and intercept of thermal decomposition and activation parameters of complex **1**

Step	*Coats-Redfern* equation			
	n	*r*	slope	intercept
1st	0	0.99913	−3.6504	−1.7687
	0.5	0.99971	−3.9821	−0.7056
	1	0.99995	−4.3442	−0.45176
2nd	0	0.99398	−4.9962	−1.9771
	0.5	0.99456	−5.3358	−1.1172
	1	0.9949	−5.6908	−0.2188
3rd	0	0.9873	−5.1494	−5.2832
	0.5	0.9903	−5.5653	−4.4901
	1	0.9927	−6.003	−3.6554
4th	0	0.98784	−14.832	−3.9519
	0.5	0.98955	−15.9823	−5.4791
	1	0.99106	−17.1932	−7.0853

Step	$\frac{T}{K}$	$\frac{E^*}{\mathrm{kJ\,mol^{-1}}}$	$\frac{\Delta H^*}{\mathrm{kJ\,mol^{-1}}}$	A	$\frac{\Delta S^*}{\mathrm{kJ\,K^{-1}\,mol^{-1}}}$	$\frac{\Delta G^*}{\mathrm{kJ\,mol^{-1}}}$
1st	346	46.12	33.23	1352.9	−0.187	97.79
2nd	446	47.32	43.59	901.44	−0.192	129.09
3rd	671	53.11	47.51	69.52	−0.216	192.83
4th	861	142.95	135.48	3.8×10^8	−0.128	245.8

state. Based on the data of thermal analysis, the decomposition of mononuclear and binuclear complexes can be represented as shown in Schemes 1 and 2.

IR Spectra

In order to ascertain the mode of bonding of the ligand to the metal ions, a careful comparison of the IR spectra of the ligand and its metal complexes was considered. The IR spectral bands of diagnostic importance are given in Table 5. The presence of water molecules leads to intense ν_{OH} absorption bands in the 3380–3400 cm^{-1} region. The coordination of water molecules is supported by the presence of the new band at 805–810 cm^{-1} for all complexes, which is assigned to the out of plane deformation vibration γ_{OH} of coordinated water molecules [17, 18].

The ν_{C-N} band at 1310 cm^{-1} was shifted to lower wavenumbers denoting the coordination of the amino nitrogen atom to the metal ions. The bands due to the phenolic OH-groups (δ_{OH} at 1220 cm^{-1} and υ_{C-OH} at 1090 cm^{-1}) in the IR spectrum of the ligand vanished completely from the spectra of the 2:1 complexes whereas in the spectra of the 1:1 complexes these bands were shifted to lower wavenumbers and their intensity decreased largely. This indicates the displacement of the phenolic protons by the metal ions.

Table 4. Values of correlation coefficient, slope, and intercept of thermal decomposition and activation parameters of complex **3**

Step	*Coats-Redfern* equation			
	n	*r*	slope	intercept
1st	0	0.9822	−3.5526	−2.5652
	0.5	0.9897	−4.0899	−0.8835
	1	0.9949	−4.6937	−1.0002
2nd	0	0.9952	−7.4749	3.0224
	0.5	0.9984	−8.3455	5.0736
	1	0.9997	−9.3214	7.3685
3rd	0	0.9984	−5.5284	−4.5202
	0.5	0.9973	−6.2994	−3.0741
	1	0.9928	−7.1771	−1.4334
4th	0	0.9944	−11.302	1.293
	0.5	0.9988	−13.111	3.9471
	1	0.9975	−15.280	7.1201

Step	$\frac{T}{K}$	$\frac{E^*}{\text{kJ mol}^{-1}}$	$\frac{\Delta H^*}{\text{kJ mol}^{-1}}$	A	$\frac{\Delta S^*}{\text{kJ K}^{-1}\text{ mol}^{-1}}$	$\frac{\Delta G^*}{\text{kJ mol}^{-1}}$
1st	354.3	39.03	36.07	2497.7	−0.181	100.3
2nd	472.9	77.5	73.56	2.73×10^8	−0.126	132.9
3rd	593	45.97	41.02	12.74	−0.229	177.1
4th	792.4	114.44	107.83	3.49×10^5	−0.147	224.3

The $\nu_{C=O}$ bands of the carboxyl groups are located at 1750, 1660, and 1640 cm^{-1} in the spectrum of the ligand. On the other hand, these bands changed to a peak at 1745 cm^{-1} and two peaks at 1610 and 1590 cm^{-1} in the spectra of 2:1 complexes whereas for the 1:1 complexes the carboxylate bands were observed at 1745 and 1600 cm^{-1}. This reveales the contribution of one carboxyl group to complexation with each metal ion.

The IR spectra of all complexes display two new bands at 460–475 and 370–385 cm^{-1}, which can be assigned to the stretching modes of *M*–O and *M*–N bonds formed in the complex. Accordingly, the *PhP* ligand seems to act as a dibasic tridentate ligand coordinated to each metal ion *via* the N-atom and the phenolate and carboxylate oxygen atoms.

Magnetic Measurements and Electronic Absorption Spectra

The magnetic moment values (Table 1) are 5.8 and 5.2 BM for complexes **1** and **2**, respectively. The lower value for complex **2** found at 5.2 BM because the antiferromagentic interaction is not possible for complex **1** [19]. The electronic spectra of Mn(II) complexes **1** and **2** exhibit two bands (Table 5), the first one at 16949 and 17241 cm^{-1} for complexes **1** and **2**, respectively, which can be assigned to $^6A_{1g} \longrightarrow {}^4T_{1g}$ (4G). The second band at 26316 and 26667 cm^{-1} is

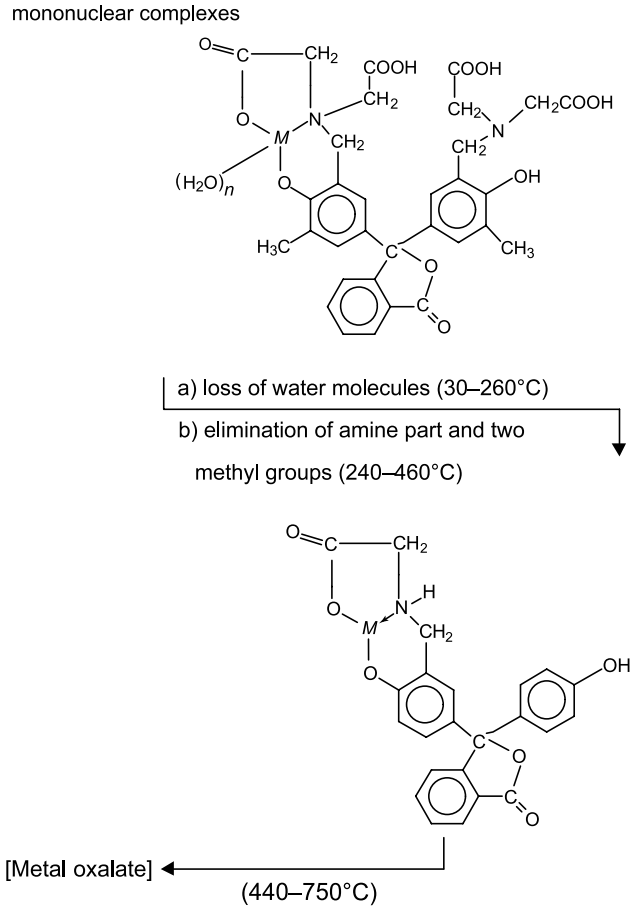

Scheme 1

assigned to $^6A_{1g} \longrightarrow {}^4E_g$ (4G). These bands correspond to octahedral geometry around Mn(II) ion [20, 21].

The magnetic moment values of the Co(II) complexes **3** and **4**, are consistent with the tetrahedral environment [22]. The lower μ_{eff} value for binuclear complex **4** than the mononuclear **3** can be explained by the existence of Co(II)–Co(II) interaction in the solid lattice. The Nujoll mull spectra of Co(II) complexes **3** and **4** show bands at 17543 and 17391 cm^{-1} which can be assigned to $^4A_2 \longrightarrow {}^4T_{1g}$ (P) transition in a tetrahedral geometry [19].

The diamagnetic nature of the Ni(II) complexes indicates the square planar geometry around Ni(II) ion. The electronic spectra of Ni(II) complexes **5** and **6** exhibit one characteristic band at 19230 and 18348 cm^{-1}, respectively, which can be assigned to $^1A_{1g} \longrightarrow {}^1B_{1g}$ transition in a square planar geometry [23–25].

For Cu(II) complexes **7** and **8**, the electronic absorption spectra show one band at 17242 and 17857 cm^{-1}, respectively, which can be assigned to $^2B_{lg} \longrightarrow {}^2E_g$ transition. The position of these bands suggests a square planar stereochemistry for such complexes. The Cu(II) complexes **7** and **8** exhibit magnetic moments (Table 1) close to the spin value for only one unpaired electron (1.74 and 1.63 BM) at room

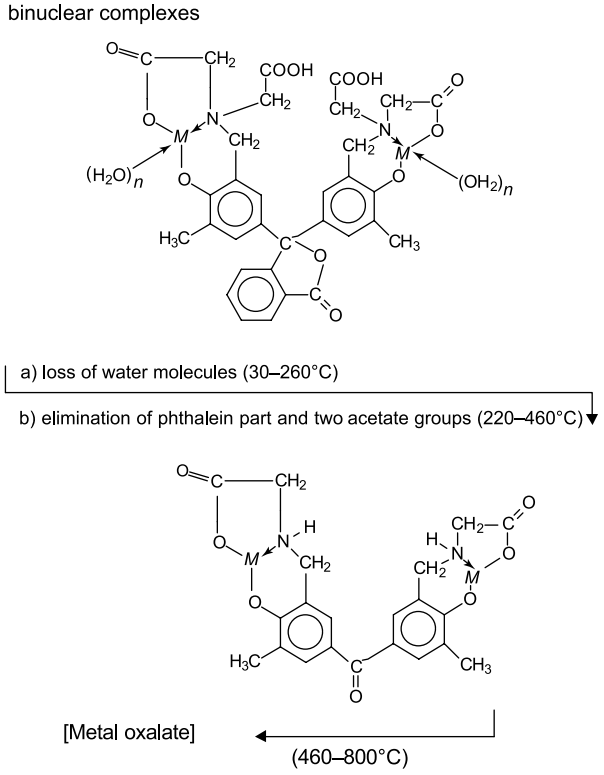

Scheme 2

temperature. The lower magnetic moment for the binuclear complex can be attributed to antiferromagnetic interaction between Cu(II) ions in the complex [19].

ESR Spectra

The powder X-band ESR spectra of the Mn(II), Co(II), and Cu(II) complexes were recorded at 293 K for Mn(II) and Cu(II) and at 93 K for Co(II) compounds. The g_{eff} values are depicted in Table 1, and representative spectra are given in Fig. 3.

The spectra of the Mn(II) complexes exhibit broad isotropic signals showing the sixtet fine structure characteristic of d^5 Mn(II) ions. The g_{eff} values of the mononuclear and binuclear complexes are not much different.

The spectra of the Co(II) complexes at 93 K display a very broad signal with no hyperfine structure. The broadening of the signal and absence of hyperfine structure can be ascribed to the existence of the metal ions in non equivalent lattice positions [26]. The g_{eff} value (Table 1) of the mononuclear complex is lower than that for the binuclear one. This can be attributed to the lateral interaction between the two metal cations.

The spectra of the Cu(II) complexes show isotropic broad lines indicating the absence of axial ligands, also the equatorial Cu–O distances would probably be not much different. The ESR patterns together with the g_{eff} values for the Mn(II), Co(II), and Cu(II) complexes under study reveal that the Mn(II) acquires octahedral geometry whereas the Co(II) is tetrahedral and Cu(II) has the square planar

Table 5. IR, electronic spectra, and electrochemical study data

No.	IR data (cm^{-1})						
	υ_{OH}	$\upsilon_{C=O}$	$\upsilon_{C=O}$	$\upsilon_{C=O}$	υ_{M-H_2O}	υ_{M-O}	υ_{M-N}
L	3430(s) 3250(m)	1750(b)	1660(s)	1620(s)	–	–	–
1	3400(s) 3210(s)	1745(m)	1660(m)	1610(m)	810(m)	475(m)	380(m)
2	3390(s)	1740(b)	1610(s)	1590(s)	805(m)	465(m)	370(m)
3	3400(b) 3200(m)	1745(b)	1660(s)	1590(s)	810(s)	475(m)	375(m)
4	3400(b)	1745(b)	1610(s)	1595(s)	805(m)	465(m)	370(w)
5	3400(b) 3200(b)	1745(b)	1660(b)	1590(s)	805(m)	465(m)	380(m)
6	3380(b)	1745(b)	1620(s)	1590(s)	805(s)	470(m)	385(m)
7	3300(b) 3200(s)	1740(b)	1660(s)	1600(s)	810(s)	465(m)	380(m)
8	3380(b)	1750(b)	1610(s)	1590(s)	810(s)	460(m)	385(w)

No.	Electronic spectra (cm^{-1})	Electroreduction data		
		$\frac{E^{l}_{1/2}}{v}$	$\frac{E^{e}_{1/2}}{v}$	$\frac{E_p}{v}$
L	–	–	–	–
1	29412, 16949	−1.51	–	−1.53
2	26667, 17094	–	–	–
3	17543	−1.20	1.36	1.42
4	17391	−1.20	1.35	1.38
5	25974, 19230, 16129	−1.10	−1.20	−1.05
6	25974, 18348, 16000	–	–	–
7	25974, 17094	+0.04	−0.11	−0.37
8	24390, 17241	–	–	–

(b) = broad, (s) = strong, (m) = medium, (w) = weak, $E^{l}_{1/2}$ = literature data (Ref. [28]), $E^{e}_{1/2}$ = half wave potentials at DME *vs*. SCE, E_p = peak potential *vs*. 0.1 *M* Ag/AgCl electrode

distribution. The g_{eff} values for the Co(II) and Cu(II) complexes are higher than that of the free electron (2.0023). According to *Fidone* and *Stevens* [27], the positive contribution to the g_{eff} values indicates an increased covalent character in the mode of the ligand to metal bonding.

Electrochemical Studies of the Complexes

The electroreduction of the metal chelate under study was carried out applying DC polarography at *DME* using 0.1 *M* KCl solution containing 30% (*v*/*v*) *DMF* as a supporting electrolyte. The polarogram of each complex consists of a single irreversible wave involving two electrons corresponding to the reduction of the

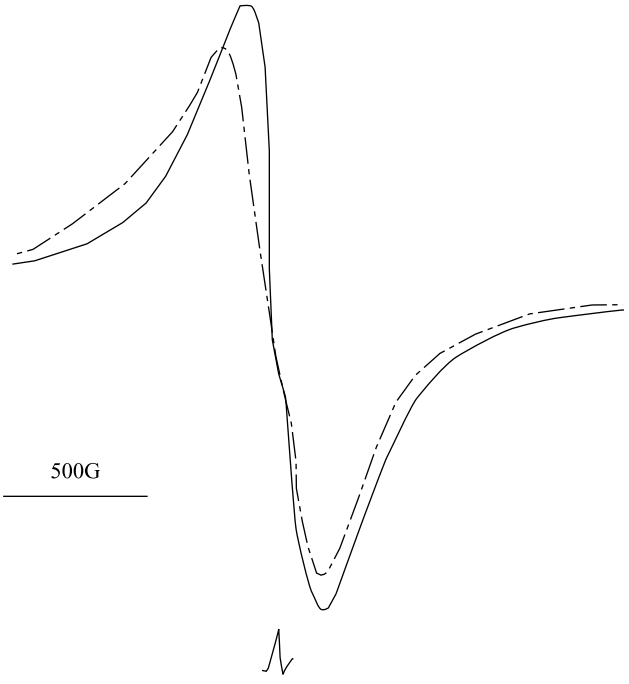

Fig. 3. X-band ESR spectra of mononuclear and binuclear Mn(II) complexes

mononuclear complexes

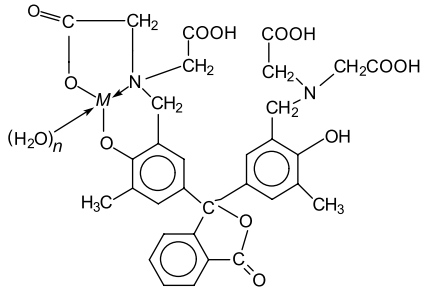

$n = 1$ for $M =$ Co, Ni, and Cu, $n = 3$ for $M =$ Mn; the geometry for Co(II) complex is tetrahedral, for Ni(II) and Cu(II) complexes is square planar, and for Mn(II) complex is octahedral

binuclear complexes

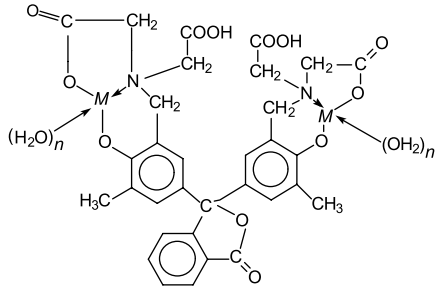

$n = 1$ for $M =$ Co, Ni, and Cu, $n = 3$ for $M =$ Mn; the geometry for Co(II) complex is tetrahedral, for Ni(II) and Cu(II) complexes is square planar, and for Mn(II) complex is octahedral

Scheme 3

metal ion to the metallic state ($M^{+2} + 2e^- \rightarrow M^0$). The waves of Cu(II) complexes are well defined with $E_{1/2} = -0.11$ V, whereas for the other metal ion complexes the waves are not well defined and join to some extent the wave due to the reduction of H^+ ions. The height of the waves for the binuclear complexes is almost double that of the mononuclear ones confirming the presence of two metal ions in such complexes.

The cyclic voltammograms of some complexes were recorded in the same medium as for DC polarography. The CV curves comprise one cathodic wave but no anodic ones indicating the irreversible nature of the electrode reaction. This finding is further supported by the shift of E_p to more negative values with increasing the scan rate.

The $E_{1/2}$ and E_p values for the complexes investigated are given in Table 5. These results indicate that the reduction of the metal ions in the complex requires higher energy than for the simple ions, which can be attributed to complex formation [28].

Based on the information gained from the various tools used in the present investigations, the bonding of the metal ions to the ligand can be formulated as shown in Scheme 3.

The structure was further supported by recording the ^{1}H NMR spectra of the diamagnetic binuclear Ni(II) complex **4**. The spectrum though was not very clean, yet it can be pointed out that it displayed signals comparable to those of the free ligand (spectra not shown), except for the lack of aromatic OH and an obvious decrease in the intensity of the carboxylic OH signals.

Experimental

All compounds used in the present study were of highest purity available from Aldrich and *BDH*. A solution of *PhP* (1 mmol in 50 cm^3 ethanol) was mixed with the metal chloride solution (1 mmol for 1:1 complexes or 2 mmol for 2:1 complexes) in 50 cm^3 50% water–ethanol mixture (v/v). The reaction mixture was freed from oxygen by purging with pure nitrogen for 30 min. The complexes started to form after reflux for 1 hour with stirring whereby the reaction mixture displayed a marked change in colour. The precipitated complex was filtered off, washed with ethanol several times, dried *in vacuo* over P_4O_{10}, and stored in a desiccator over $CaCl_2$. The yield of the reaction products is in the range 80–85%.

Elemental analysis of the solid complexes (C, H, N) were carried out in the microanalytical unit of Cairo University; their results agreed favourably with the calculated values. The metal content was determined according to the recommended procedures [29].

The IR spectra were recorded on a Perkin-Elmer model 1430 double beam spectrophotometer within 200–4000 cm^{-1} using the KBr-disc technique. Electronic spectra, as nujol mull, were obtained by the aid of a Unicam SP800 spectrophotometer. Thermal analyses were preformed on a Shimadzu-50 thermal analyzer under nitrogen atmosphere using a heating rate of 10°C min^{-1}.

Magnetic moment determination was carried out using the *Gouy* method and applying $Hg[Co(CNS)_4]$ as a standard. Diamagnetic corrections were calculated from corresponding *Pascal*'s constants.

The ESR spectra were recorded on a Joel model JES FE_2 XG spectrometer provided with an E 101 microwave bridge. The magnetic field was calibrated by a 2,2-diphenyl-1-picrylhydrazyl sample purchased from Aldrich.

The pen recording polagraph model 4001 Sargent-Welch was used for studying the polarographic behavior of the complexes under investigation. The cell described by *Meites* [30] was used for

polargraphic studies with a dropping mercury electrode (DME) ($m = 1.03\,\mathrm{mgs}^{-1}$, $t = 3.3\,\mathrm{s}$, and mercury height $h = 60\,\mathrm{cm}$) and a saturated calome electrode (SCE) as a reference electrode, supplied by Sargent-Welch.

The voltammogramms of the complexes under investigation were recorded using a potentiostate model 264 A (from EG&G). The 303 A electrode assembly was supplied by EG&G, with a hanging mercury drop electrode (area $= 2.6\times10^{-2}\,\mathrm{cm}$) as a working electrode, Pt wire as a counter electrode, and ($Ag/AgCl/KCl_s$) as a reference electrode.

References

[1] Cheng KL, Uneo K, Imamura K (1982) Handbook of Organic Analytical Reagents. CRC Press, Boca Raton, Florida
[2] Puall B, Macka M, Haddad PR (1997) J Chem A **789**: 329
[3] Toffaletti J, Kirvan K (1980) Clin Chem **26**: 1562
[4] Espersen D, Jensen A (1979) J Analytica Chimica Acta **108**: 241
[5] Kintzios S, Stvropoulou Er, Skamneli S (2004) J Plant Science **167**: 655
[6] Nesterenko P, Jones P (1996) J Liquid Chromatography & Related Technologies **19**: 1033
[7] Jones R, Foulkes M, Paul B (1994) J Chromatography A **673**: 173
[8] Paull B, Jones P (1996) J Chromatographia **42**: 528
[9] Abu EL-Wafa SM, EL-Zawawy FM, Issa RM (1983) Bull Soc Chem Belg **92**: 77
[10] Bergant F, Pacor S, Ghosh S, Chattopadhyay SK, Sava G (1993) Anti Cancer Res **13**: 1007
[11] Raman N, Kulandai Samy A, Thangaraja C, Jeysubramanian K (2003) Trans Met Chem **28**: 29
[12] Fenton DE, Lintvedet RL (1978) J Am Chem Soc **100**: 6367
[13] Gagne RR, Spiro CL, Smith TJ, Hamman CA, Thies WR, Shiemke K (1981) J Am Chem Soc **103**: 4073
[14] Urbach FL (1980) Metal Ions in Biological Systems, vol 13. Dekker, New York, p 73
[15] Nakamoto K (1970) Infrared Spectra of Inorganic and Coordination Compounds. Wiley-Interscience, New York, p 435
[16] Coats AW, Redfern JP (1964) Nature **68**: 202
[17] Gamo DM (1961) Bull Chem Soc Japan **24**: 1430
[18] Abu-El-Wafa SM, Issa RM (1990) Bull Chem Soc Fr **1**: 64
[19] Lever ABP (1984) Inorganic Electronic Spectroscopy. Elsevier, Amsterdam, p 530
[20] Chandra S, Sharma SD (2002) Transition Met Chem **27**: 732
[21] Lever ABP (1965) J Inorg Nucl Chem **27**: 149
[22] Hueso-Ureno F, Illan-Cabeza NA, Moreno-Carretero MN, Martinez-Martoz JM, Ramirez-Exposito MJ (2003) J Inorg Biochem **94**: 326
[23] Buffagni S, Vallewrino LM, Quagliano JV (1964) Inorg Chem **3**: 480
[24] Singh S, Yadava BP, Aggarawal RC (1984) Indian J Chem **23A**: 441
[25] Campbell AJM, Grazeskowi AKR (1967) J Chem Soc A 396
[26] Nataragian C, Shanthi P, Athappan P, Murugasan R (1992) Trans Met Chem **17**: 39
[27] Fidone I, Stevens KWH (1959) Proc Phys Soc (London) **73**: 130
[28] Lurie JU (1975) Handbook of analytical Chemistry (Engl Trans N Bobrov). Mir Publisher, Moscow
[29] Vogel AI (1961) Quantitative Inorganic Analysis. Longmans, London
[30] Meites L (1965) Polarographic Techniques. Interscience, New York, p 240